Chapter 2

Bayesian statistics, data sets and methodology

This chapter begins with some basic and preliminary concepts of Bayesian statistics. We provide a brief detail on the cosmological parameter estimation and the working process of the Metropolis-Hastings algorithm which is an efficient Monte Carlo Markov Chain (MCMC) technique for the parameter estimation in cosmology. Then we discuss various cosmological data from different observations that have been used in constraining the parameters of the cosmological models throughout this thesis work. We use observational data from Planck-CMB measurements, BAO measurements, H_0 measurement from Hubble space telescope (HST), and some LSS observations including Planck-Sunyeav-Zel'dovich (Planck-SZ), Canada France-Hawaii Telescope Lensing Survey (CFHTLenS), and KiDS-450. We consider different combinations of these data sets for constraining the considered models, as we will see in the forthcoming chapters. In the final section of this chapter, we discuss the methodology/codes for the data analysis used in the whole research work and the constraints on the parameters of the ΛCDM model from final Planck 2018 data.

2.1 Bayesian statistics

With the new developments in technology since the last two decades, a large amount of observational data are available with great accuracy and precision from various sources of different physical origins. This trend will be prolonged in the coming future since several surveys/experiments are currently ongoing. So it becomes important to test the viability (relevance) of constructed theoretical cosmological models against the available observational data sets. For this purpose, we use some statistical tools to extract as much information as possible about the constructed models. There are two approaches to interpret the probability in statistical analysis, namely, the frequentist school and Bayesian school. In the frequentist school of thought, the probability of an event is defined as the ratio of the occurrence of the event in a series of trials to the number of total trials in the series. In the Bayesian school of thought, the probability of an event is defined as a measure of the degree of belief about happening of the event. The main difference in two schools of thought is the way of interpreting the probability. In the frequentist school of thought, the hypotheses and the parameters of the model remains fixed whereas in the Bayesian approach the probability can be updated with the new information and it depends on the prior knowledge of the model parameters such as from previous experiments/surveys or a personal point of view. We follow the Bayesian approach in the work done in this thesis. For more details about Bayesian statistics in context of cosmology, see [57–60].

2.1.1 Estimation of parameters

The key quantity in Bayesian statistics is the likelihood function usually denoted by $\mathcal{L}(\mathbf{d}|\boldsymbol{\theta}, \mathcal{M})$ for the given data $\mathbf{d} = \{d_1, d_2, d_3, \ldots, d_n\}$ and a given model $\mathcal{M}$ which takes the parameter values $\boldsymbol{\theta} = \{\theta_1, \theta_2, \theta_3, \ldots, \theta_m\}$. Assuming that the data measurements are normally distributed about their mean values, the likelihood function up to the

proportionality is defined as

$$\mathcal{L}(\mathbf{d}|\boldsymbol{\theta}, \mathcal{M}) \propto \exp\left(-\frac{\chi^2(\boldsymbol{\theta})}{2}\right). \tag{2.1}$$

Under the assumption that the given model is true, the probability density function, $P(\boldsymbol{\theta}|\mathbf{d}, \mathcal{M})$ of parameter $\boldsymbol{\theta}$ of model $\mathcal{M}$, given data $\mathbf{d}$, is related to likelihood via Bayes' Theorem

$$P(\boldsymbol{\theta}|\mathbf{d}, \mathcal{M}) = \frac{P(\mathbf{d}|\boldsymbol{\theta}, \mathcal{M})P(\boldsymbol{\theta}, \mathcal{M})}{P(\mathbf{d}, \mathcal{M})}, \tag{2.2}$$

where the quantity on left side of eq. (2.2) is called the posterior probability ('posterior' in short) of the parameter $\boldsymbol{\theta}$, representing our degree of belief on the model parameter values after we have seen the data $\mathbf{d}$. On the right hand side, the first term in numerator is the likelihood function, $P(\mathbf{d}|\boldsymbol{\theta}, \mathcal{M})$, usually denoted by $\mathcal{L}(\boldsymbol{\theta})$, in short and gives the probability of data, given the values of the parameters. The quantity $P(\boldsymbol{\theta}, \mathcal{M})$ denotes the prior probability distribution of the parameter $\boldsymbol{\theta}$, and represent our belief about parameter values before we observed the data. This quantity quantifies our existing knowledge on parameter which may be based on past experiments/surveys or on theoretical predictions, and thus play a significant role in estimation of posterior probability. There is no general rule for choosing the prior on parameters, and in general the choice of prior falls in three categories: flat prior, Gaussian prior, and Jeffrey prior. The quantity $P(\mathbf{d}, \mathcal{M})$ in denominator of eq. (2.2) is marginal likelihood or the evidence. It has no role in parameter estimation, and it acts as normalizing constant but plays a significant role in Bayesian model selection. In the whole work of this thesis, we have used the flat prior on all the model parameters. For a particular parameter, say θ_i, defined in the range [a, b], the flat prior is given as

$$p(\theta_i) = \begin{cases} \frac{1}{a-b}, & a \leq \theta_i \leq b \\ 0, & \text{elsewhere} \end{cases} \tag{2.3}$$

Thus, in the case of flat prior on parameters, Bayes' theorem (2.2) can be used to write the posterior probability as follows:

$$P(\boldsymbol{\theta}|\mathbf{d}, \mathcal{M}) \propto P(\mathbf{d}|\boldsymbol{\theta}.\mathcal{M}) \tag{2.4}$$

Therefore, in case of flat prior choice on the model parameters, the posterior probability information can be achieved directly from the likelihood function.

2.1.2 Monte Carlo Markov Chain technique

When the number of parameters in a cosmological models become large, which is usually the case when considering the extension of the well-known standard model or when using the observational data containing supporting nuisance parameters (for example, when using full Planck-CMB data), the evaluation of full likelihood function and hence the posterior by the usual methods, such as the grid one are not efficient due to the requirement of huge amount of computation time. In such situations, the MCMC methods are good choices which converge to the region in the parameter space where the likelihood function attains maximum value. A full description of these methods can be seen in [61, 62]. The MCMC methods are efficient to generate a collection of points in the parameter space that sample the likelihood function (i.e. the target density), and consequently the posterior probability. It selects the random candidate point in parameter space in Markovian manner, i.e., the choice of next candidate point is relying only on the current candidate point, not on the previous sample history. Once the sample for the posterior using MCMC is obtained, one can calculate various quantities of interest like mean, variance, and standard deviation, etc. MCMC starts with an initial candidate point $\boldsymbol{\theta}$ with the target density $p(\boldsymbol{\theta})$, and chooses a next candidate point, $\boldsymbol{\theta}^{\star}$ with target density value, $p(\boldsymbol{\theta}^{\star})$. Then the acceptance of this new candidate point depends on the ratio of the new and old target density values. The probability distribution which generates a new candidate point for the chain on the basis of present candidate point, is usually known as proposal distribution, $q(\boldsymbol{\theta}^{\star}|\boldsymbol{\theta})$. In most of the cases the proposal distribution is

considered as Gaussian since it matches to the target distribution. A reversible proposal distribution $q(\boldsymbol{\theta}|\boldsymbol{\theta}^{\star})$ can also be defined in a similar manner, which gives a distribution to reverse the chain. The simplest algorithm which is widely used in MCMC technique in cosmology is the Metropolis-Hastings (M-H) algorithm [63], based on the Bayesian statistical approach. In this algorithm, the probability of acceptance of the new candidate point is given as

$$p(\mathrm{acceptance}) = \min\left(1, \frac{\mathrm{p}(\boldsymbol{\theta}^{\star})\mathrm{q}(\boldsymbol{\theta}^{\star}|\boldsymbol{\theta})}{\mathrm{p}(\boldsymbol{\theta})\mathrm{q}(\boldsymbol{\theta}|\boldsymbol{\theta}^{\star})}\right). \tag{2.5}$$

In case of symmetric proposal distribution, i.e., $q(\boldsymbol{\theta}^{\star}|\boldsymbol{\theta}) = q(\boldsymbol{\theta}|\boldsymbol{\theta}^{\star})$, that means the chain is reversible. This algorithm is simply known as Metropolis instead of Metropolis-Hastings, and has the following form:

$$p(\mathrm{acceptance}) = \min\left(1, \frac{\mathrm{p}(\boldsymbol{\theta}^{\star})}{\mathrm{p}(\boldsymbol{\theta})}\right). \tag{2.6}$$

The acceptance or rejection of the new candidate point is decided by generating a random number, say u, from the uniform distribution $[0, 1]$. The new point will be accepted as a sample point if $u < p(\mathrm{acceptance})$, otherwise it will be rejected. It is clear from eq. (2.6) that if the new point $\boldsymbol{\theta}^{\star}$ has target density $p(\boldsymbol{\theta}^{\star})$ higher than the target density $p(\boldsymbol{\theta})$ of the present point $\boldsymbol{\theta}$, the new point will always be accepted. However, if the target density of the new point is smaller than the target density of the current point, then the new point might be accepted or not. If the new point is accepted, then it will be added to the chain and move for the next point. If the new point is rejected, the process will be repeated. The MCMC methods play a significant role in cosmology, and are generally applied in the observational data analysis using the well-known software such as CosmoMC [64] and Monte Python [65], which are particularly designed for cosmology and astrophysics. The CosmoMC is written in Fortran language and interfaced with Boltzmann solver code CAMB [66]. The Monte Python [65] code is written in Python as its name indicates and interfaced with another Boltzmann solver code CLASS [67]. The working process of both CosmoMC and Monte Python is based on the Metropolis-Hastings algorithm. The

subsection (2.3.1) describes the Monte Python and CLASS codes with some more details.

2.1.3 Bayesian model selection

After performing the parameter estimation on the considered model, the next task is to test the statistical goodness of the model by comparing it with the well-known standard model. There are two distinct tools for doing the same. One is based on Bayesian inference such as Bayesian evidence and an approximation of it is called Bayesian Information Criterion (BIC). The other is based on Information theory such as the Akaike Information Criterion (AIC). There is also an additional information criterion, Deviance Information Criterion (DIC) which inherits the properties from both, information theory and Bayesian methods. It is important to mention that the AIC can be derived in a Bayesian way and BIC can be derived in a non-Bayesian way, as argued in [68]. Therefore, one should not think the argument about using AIC versus BIC as a Bayesian versus frequentist approach. One natural question that immediately comes in mind is that which one is better among these possible model selection tools. Here, we will restrict ourselves and not discuss the advantage of one over another tool. For most cosmologists, the Bayesian evidence is the preferred tool but the problem with the Bayesian evidence is in the estimation of multidimensional integral which requires a lot of numerical computation. Although, nowadays there are available codes such as CosmoNest which makes this task easier. In the whole work of this thesis, we use a simple model selection criterion which is widely used in cosmology, astrophysics, and elsewhere. We use the Akaike information criterion, AIC [68, 69].

2.1.4 Akaike information criterion

The AIC has been widely applied in cosmological and astrophysical problems and it is relatively simple to use since it requires only the maximum likelihood function of the model. The AIC is defined as

$$\mathrm{AIC} = -2\ln\mathcal{L}_{\max} + 2N, \tag{2.7}$$

where $\mathcal{L}_{\max}$ is the likelihood function of the model evaluated at the set of model parameters which maximize the likelihood and N is the total number of free parameters in the model. Under the further assumption that the distribution of errors follows a Gaussian distribution, the above equation reduces to

$$\text{AIC} = \chi^2_{\min} + 2N, \tag{2.8}$$

where $\chi^2_{\min}$ is the usual chi-squared evaluated at the maximum likelihood estimate of the model parameters. For the statistical comparison, the AIC difference between the model under study and the reference model (the best-fit model concerning which comparison has to be done) is calculated. This difference in AIC values can be interpreted as the evidence in favor of the candidate model (the model under study) over the reference model. It has been argued in [70] that one model can be considered statistically better concerning others if the AIC difference between the two models is greater than a threshold value $\Delta_{\text{threshold}}$. According to the thumb rule of AIC, $\Delta_{\text{threshold}} = 5$ is the universal threshold value (the minimum AIC difference value [71]) to assert strong statistical support in favor of a model compared to other, regardless the properties of the model considered for comparison. Thus, an AIC difference of 5 or more between two models favors the model with smaller AIC value.

2.2 Observational data analysis

2.2.1 CMB anisotropy measurement

As mentioned in the previous chapter, the CMB radiation was first discovered by Penzias and Wilson in 1965 [72], with uniform temperature coming from all directions of the sky. Very soon with the advancement in technology, it was observed that there is a very tiny difference in the temperature of the CMB photons coming from any two random directions, called the temperature anisotropy. Many cosmologists in the 80's predicted the CMB anisotropy by looking back in time from the present observed inhomogeneous

structure to the decoupling epoch. They calculated that it should be at least of the order 10^{-6} to form clusters of galaxies observed today. At that time, due to a lack of technical instruments, the measurement of this temperature anisotropy was a challenging task among the cosmological community.

In the period of the 90's, several efforts were made via various experiments to detect the anisotropies in CMB. The first success was achieved in 1992 by the National Aeronautics and Space Administration (NASA) satellite, COsmic Background Explorer (COBE) embedded with an interferometer of great sensitivity [73]. The average amplitude of the temperature was measured as $\simeq 10^{-5}$ by the COBE satellite which mapped the anisotropies in all parts of the sky. This anisotropy measurement was in good agreement with the theoretical estimations. The angular resolution of the COBE experiment was very small (about a few degrees only), due to which anisotropies observed around one degree or less than that became smooth in the detector. Thus, COBE was successful in measuring the CMB spectrum only on those wavelengths which were larger than the sound horizon at decoupling, hence it did not provide any probe of the acoustic oscillations. After the COBE, several new experiments were designed with the high angular resolution, to measure the power spectrum at smaller wavelengths than the sound horizon at decoupling. The angular power spectrum at small wavelengths is required for observing the acoustic peaks. In 2000, the first acoustic peak was observed by two ground-based balloon experiments, namely BOOMERanG [74, 75] (a US-Italian-Canadian balloon) and MAXIMA [76, 77]. These experiments received great attention from cosmologists in the direction of CMB measurements. After COBE, the NASA satellite, Wilkinson Microwave Anisotropy Probe (WMAP) [78, 79] and the Planck satellite operated by European Space Agency (ESA) have measured CMB anisotropies. These satellite experiments have provided a high-resolution map of the full sky in addition to ground-based experiments. Nowadays, Planck is the most promising experiment which provides an excellent measurement of anisotropies in the CMB temperature.

2.2.2 Planck mission and data release

Planck experiment is designed for the measurement of spectra of anisotropies in CMB up to a percent level of accuracy and precision. It was started on 14th May 2009, and it continuously observed the whole sky from 2009 to 2018. The final Planck CMB 2018 data is released, and this mission is over. The whole data sets together with various other things like source catalogs and CMB maps are publicly available for users. These can be extracted from the Planck Legacy Archive website [80]. For more details about the Planck mission, its main goal and technical instrumentation, see the recent article [81].
Planck Collaboration regularly releases the data and a series of associated papers. Its first release of data and related papers came in 2013 [82, 83]. The constraints on standard cosmological parameters as well as the other various derived parameters and their related physics can be seen in [84]. Planck collaboration released second data and related papers in 2015 [85]. In this release, the E-mode polarization through the TE cross-correlation and the EE auto-correlation spectra were included in the likelihood [86], and hence the cosmological results and power spectra were improved [32]. The final results from the full Planck mission were released in 2018 [87]. In this release, the reionization optical depth was measured with high precision as compared to Planck 2015 results, due to the improved measurements of polarization on large scale. This precise measurement of optical depth significantly improved the constraints on other correlated parameters [88]. The likelihood codes of the final Planck mission were not publicly available during the preparation of this thesis. A list of Planck collaboration publications: including Planck 2018 results, Planck 2015 results, Planck 2013 results, Planck intermediate, and early results, and many others can be found at [89]. It is important to mention that some cosmological parameters show the degeneracy (i.e., different parameters have similar effects on the CMB spectrum) with the CMB data alone. To break the parameter degeneracy, some supplementary cosmological probes such as BAO, HST, SNe Ia, etc. are usually used with CMB data. We will discuss about the supplementary data sets used in this thesis in later subsections.

2.2.3 CMB power spectrum

It is well known that the small initial perturbations in matter and radiation components have evolved from very early Universe to present observable Universe. The inhomogeneities in the matter have evolved due to the gravitational instabilities in matter distribution and formed the observed structures in the Universe such as galaxies, galaxy clusters, superclusters, etc. The same initial fluctuations have also created the anisotropies in the radiation which we observe today in the CMB radiation coming from all parts of the sky. Since the photons energy density, (hence the fluctuations in it) is related to the temperature via $\rho_\gamma \propto T^4$. Thus, by measuring the temperature across the whole sky one can easily find the anisotropies in the CMB photons [1]. The temperature anisotropy of photons can be defined as

$$\Theta(\hat{n}) = \frac{T(\hat{n}) - \bar{T}}{\bar{T}}, \tag{2.9}$$

where Θ is the temperature perturbation, $\hat{n}$ denotes the unit vector along the line of sight, and $\bar{T}$ denotes the temperature of CMB, which is determined by averaging the temperature on the sky from all directions. It is given as

$$\bar{T} = \frac{1}{4\pi} \int d\Omega_{\hat{n}} T(\hat{n}), \tag{2.10}$$

where $d\Omega_{\hat{n}}$ represents the infinitesimal solid angle in a direction $\hat{n}$. The temperature perturbation $\Theta(\hat{n})$ in eq. (2.9) can be expressed in terms of spherical harmonics, Y_{lm} as follows:

$$\Theta(\hat{n}) = \sum_{l=0}^{\infty} \sum_{m=-l}^{l} a_{lm} Y_{lm}(\hat{n}), \tag{2.11}$$

where a_{lm}'s are the complex constant coefficients. With the help of basic definitions and relations of spherical harmonics with Legendre polynomials, the a_{lm}'s can be expressed in terms of temperature multipoles, Θ_l, as follows:

$$a_{lm} = -(i)^l \int \frac{d^3\vec{k}}{2\pi^2} Y_{lm}(\hat{k}) \Theta_l(t_0, \vec{k}), \tag{2.12}$$

where $\hat{k}$ stands for unit wave vector. The spherical harmonics can be interpreted physically as the angular scale $\theta \sim \pi/l$. They can be modeled as the Fourier series over the surface of a sphere. Thus, a particular value of l represent the function over a particular portion on the sphere, for instance, $l = 0$ refers to a function on the whole sphere, $l = 1$ over the three axes of the sphere and so on. Thus, for large l, spherical harmonics vary on small scales, and a_{lm}'s describe the amplitude of temperature fluctuations at each location in the Universe. It is also known that the mean of the temperature fluctuations over the whole sky vanishes. So the quantity of interest which needs to be estimated is the variance which does not vanish. The two-point correlation function of the a_{lm} can be expressed in terms of the primordial curvature power spectrum:

$$\langle a_{lm} a_{l'm'} \rangle = \delta_{ll'} \delta_{mm'} \left[\frac{1}{2\pi^2} \int \frac{dk}{k} \Theta_l(t_0, k) \mathcal{P}_{\mathcal{R}}(k) \right], \tag{2.13}$$

which represents that average has been taken over many realizations of random processes. The term given in square bracket is the theoretical angular power spectrum, C_l which is only function of multipoles l, not of the orientation m due to the statistical isotropy. The theoretical angular power spectrum can be written as follows

$$C_l = \frac{1}{2\pi^2} \int \frac{dk}{k} \Theta_l(t_0, k) \mathcal{P}_{\mathcal{R}}(k). \tag{2.14}$$

This C_l is of great importance and provides all necessary information about a model of the Universe which is contained in the temperature map of CMB. The relation between the measured temperature fluctuation or perturbation, $\Theta(\hat{n})$ and the angular power spectrum, C_l is given as follows:

$$\langle \Theta(\hat{n}) \Theta(\hat{n}') \rangle = \sum_{l=0}^{\infty} \frac{(2l+1)}{4\pi} C_l \mathcal{P}_l(\hat{n}.\hat{n}'), \tag{2.15}$$

where $\mathcal{P}_l(\hat{n}.\hat{n}')$ are the Legendre polynomials. Since we have observations of anisotropies of CMB only in one realization (i.e., in our observable Universe), it is natural to expect

that the observed power spectrum will differ from the theoretical one which is averaged over many realizations. Hence, the square $|a_{lm}|^2$ will not be exactly equal to C_l and there should be some scattering around C_l. The scattering around C_l can be reduced considerably because for any fixed l, the statistical distribution of $|a_{lm}|^2$ does not depend on the orientation, m. Hence, for any fixed l, the quantity which should be very closer to underlying C_l is the average of all observed coefficients $|a_{lm}|^2$, given as

$$C_l^{\rm obs} = \frac{1}{(2l+1)} \sum_{m=-l}^{l} |a_{lm}^{\rm obs}|^2. \tag{2.16}$$

It is easy to show that for Gaussian a_{lm}'s

$$\langle (C^{\rm obs} - C_l)^2 \rangle = \frac{C_l^2}{2l+1}. \tag{2.17}$$

This reveals a fundamental uncertainty (scattering) between the theoretical and observed C_l's. This is called the cosmic variance. For small values of l, variance would be large which means that shape of the true underlying C_l's is not precisely known at low multipoles. See the CMB temperature power spectra in Figure 2.1 which is extracted from final Planck-CMB 2018 results [88]. All length scales on CMB are quantified by the wave number k, so instead of using $\Theta(\hat{n})$, it is useful to consider $\Theta(k)$, which is the Fourier transform of $\Theta(\hat{n})$. Therefore, in the Fourier space the power spectrum can be expressed as follows

$$\begin{aligned} \langle \Theta(k)\Theta(k') \rangle &= \int \frac{d^3k}{(2\pi)^3} \int \frac{d^3k'}{(2\pi)^3} \langle \xi(k)\xi(k') \rangle |T_l(k)|^2 \\ &= \int \frac{d^3k}{(2\pi)^3} \mathcal{P}_\prime(k) |T_l(k)|^2, \end{aligned} \tag{2.18}$$

where $\xi(k)$ is the initial condition and $T_l(k)$ is the transfer function, solution to the evolution equation of density of each component of the Universe. The second line follows from two point correlation, $\langle \xi(k)\xi(k') \rangle = (2\pi)^3 \mathcal{P}_\mathcal{R}(k) \delta^3(k-k')$, where $\mathcal{P}_\mathcal{R}(k)$ is the primordial power spectrum. It involves just two perturbative parameters, namely, the amplitude

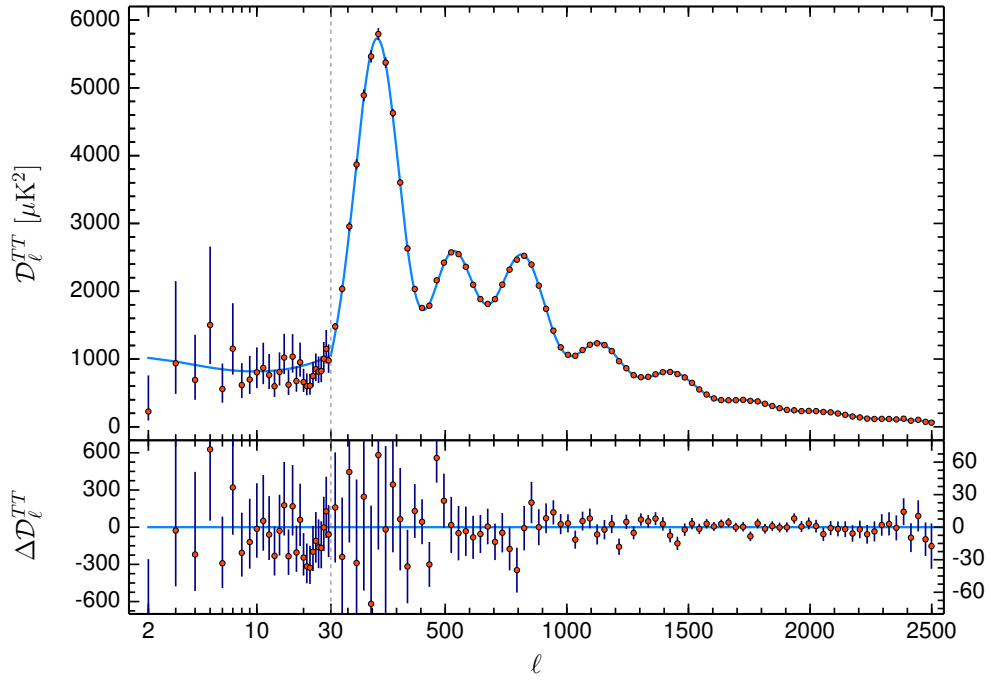

Figure 2.1: CMB temperature power spectrum from Planck-2018 data. The blue line shows theoretical ΛCDM spectrum from Planck TT, TE, EE + lowE + lensing likelihoods in the upper panel. In the lower panel residual is shown with respect to ΛCDM.

of scalar perturbation A_s and the spectral tilt n_s. It is expressed as follows

$$\mathcal{P}_{\mathcal{R}}(k) = A_s \left(\frac{k}{k_\star}\right)^{n_s - 1}, \tag{2.19}$$

where $k_\star$ stands for pivot scale at the time of recombination. If $n_s = 1$, then spectrum is called scale invariant in which case the primordial power spectrum will give only a shift in the amplitude of power spectrum of CMB. In the case, when $n_s \neq 1$, the tilting in primordial power spectrum can influence the scale dependence in the power spectrum of CMB. After equating eq. (2.18) to the Fourier transform of eq. (2.15) and then integrating over all angles on the sky, we find the connection between the C_l and transfer function of the photon,

$$C_l = \frac{2}{\pi} \int dk k^2 \mathcal{P}_{\mathcal{R}}(k) |T_l(k)|^2. \tag{2.20}$$

The calculation of the CMB power spectrum needs a highly complex numerical code to include various physical processes that occurred when CMB formed. There are some numerical codes available, like CAMB, CLASS, etc. which can be used to calculate the temperature power spectrum. The characteristic features of the power spectrum depend on the provided initial conditions at the time of CMB production. These features also depend on the energy content available before and after the recombination. Thus, the CMB power spectrum not only contains the information of the very early Universe but also provides a way to estimate the current amount of matter-energy contents present in the Universe today. Various possible effects of the cosmological parameters on the spectra can be easily explained with the understanding of the evolution of the perturbations with a background FLRW cosmology.

2.2.4 Matter power spectrum

The matter power spectrum describes the density contrast, i.e., the difference between the local density and average density of the Universe. The matter power spectrum is different from the CMB power spectrum with the fact that there is no competitive force (like radiation pressure in case of CMB spectrum) to counteract the gravitational force of matter. Due to this reason, there is no oscillatory pattern in the matter power spectrum, and it is a smooth curve for the variations of galaxies counts on different length scales. The matter power spectrum can be defined as the Fourier transform of the two-point correlation function of matter density. The two-point correlation function can be defined as the probability of relating a function, say in our case the density perturbation, δ_m to another function, δ'_m at a spatial distance $\vec{x}$. It is usually denoted by $\langle \delta_m \delta'_m \rangle$, and defined as

$$\xi(\vec{x}_1, \vec{x}_2) = \langle \delta_m(\vec{x}_1) \delta'_m(\vec{x}_2) \rangle, \tag{2.21}$$

where the average is taken over a large number of such configurations in space. It is positive if the density perturbation is expected to have the same sign at both locations, $\vec{x}_1$ and $\vec{x}_2$, and negative for an overdensity at one and under density at the other. Thus

it probes how density fluctuations at different locations are correlated with each other. Due to statistical homogeneity, $\xi(\vec{x}_1, \vec{x}_2)$ does not depends on individual points, but on the difference of coordinates $\vec{x}_1 - \vec{x}_2$ of random locations. Thus, the correlation function depends only on the length scale of interest, not on location and direction. The power spectrum of density fluctuation δ_m is defined as follows:

$$\langle \delta_m(t, \vec{k}) \delta_m^\star(t, \vec{k'}) \rangle = \delta_D(\vec{k} - \vec{k'})\, P(t, k), \tag{2.22}$$

where δ_D is the 3D dirac delta function which is constrained by $\vec{k} = \vec{k'}$, and $P(t, k)$ is the matter power spectrum of $\delta_m(\vec{x})$ which is function of magnitude of wave vector due to statistical isotropy. From eq. (2.22), it is clear that if there are lots of very over and under dense regions in the matter distribution, the power will be large and in case of smooth distribution it will be small. Under the assumption of Gaussian initial conditions and up to the limit where perturbations remain linear, the power spectrum at a given time can be expressed as a product of primordial spectrum and square of the relevant transfer function. Assuming a power-law primordial spectrum, the power spectrum can be given as

$$P(t, k) = \frac{2\pi^2}{k^3}\, A_s \left(\frac{k}{k^\star}\right)^{n_s - 1} \delta_m^2(t, k), \tag{2.23}$$

where $\delta_m(t, k)$ is called transfer function. Hence the evolution of transfer function provides us the cosmological information encoded in the matter power spectrum. Figure 2.2 (extracted from [90]) shows the power spectrum of galaxy distribution. There are deviations in the curve which indicate that dynamics of the Universe have changed with time. Also, we can see that at large scales (small values of k), fluctuations are very weak which means that galaxy distribution is very close to homogeneous. The power spectrum has dimension of $(\mathrm{length})^3$ (or k^{-3}), most often it is written in the combination $k^3 P(k)/2\pi$ which is a dimensionless quantity indicating clumpiness on scale k.

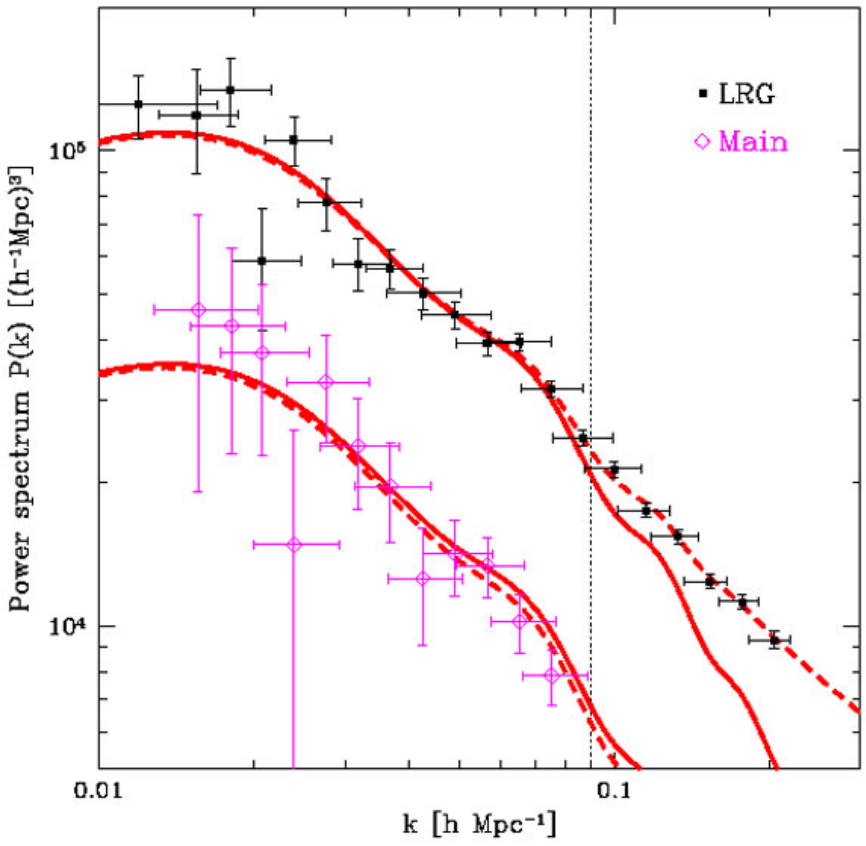

Figure 2.2: Matter power spectrum from luminous red galaxies SDSS sample (in black color) and the main SDSS sample (in magenta color). Solid and dashed lines respectively denote the theoretical prediction for ΛCDM model and non-linear corrections. The onset of non-linear corrections is clearly visible for $k \gtrsim 0.09$ h/Mpc (vertical line).

2.2.5 Baryonic acoustic oscillations measurements

BAOs are the acoustic waves in the tightly coupled photon-baryon fluid before the time of recombination. Before recombination, due to the Thomson scattering between photons and baryons, they were tightly coupled to each other. The competition between photons pressure and gravity of baryons leads to acoustic waves, which have traveled in plasma till the time of recombination. Once the photons decoupled from the baryons just after recombination, they have propagated freely in the remaining expansion history of the Universe, and thus carry the information of very early Universe. The distance traveled by acoustic waves before the time of recombination (where they have frozen) set a char-

acteristics scale in the distribution of perturbations, which we call sound horizon. These waves leave imprints in the distribution of radiation, seen today as anisotropies in CMB, and also in the clusters of galaxies. This was first detected by authors in [91] in 2005 and since then BAOs are accepted as one of the major independent probes in the observational cosmology. The BAO signal has been further measured by different redshift surveys such as Six-Degree Field Galaxy Survey (6dFGS), SDSS, and Baryonic Oscillations Spectroscopy Survey (BOSS), etc. These survey estimate the following distance ratio

$$\xi = \frac{r_s(z_{\rm drag})}{D_v(z)}, \tag{2.24}$$

where $r_s(z_{\rm drag})$ denotes the comoving sound horizon at drag epoch (i.e., when baryons became dynamically decoupled from photons), and is defined as

$$r_s(z_{\rm drag}) = \int_{z_{\rm drag}}^{z_{\rm ini}} c_s^2 \frac{dt}{a}. \tag{2.25}$$

$D_v(z)$ is defined in such a manner that it will be suitable for the analysis of spherically averaged two point statistics,

$$D_v(z) = \left((1+z)^2 \, cz \frac{d_A^2(z)}{H(z)} \right)^{1/3}, \tag{2.26}$$

where $d_A(z)$ is the angular diameter distance defined as

$$d_A(z) = \frac{c}{1+z} \int_0^{z_{\rm dec}} \frac{dz'}{H(z)}. \tag{2.27}$$

The BAO measurements are normally given in form of the ratio $r_s(z_{\rm drag})/D_v(z_{BAO})$. Here, we use four probes of BAO measurements: the Six Degree Field Galaxy Survey (6dFGS): $r_s/D_v(z_{\rm eff} = 0.106) = 0.327 \pm 0.015$ [92], the Main Galaxy Sample of Data Release 7 of Sloan Digital Sky Survey (SDSS-MGS): $D_v(z_{\rm eff} = 0.15)/r_s = 4.47 \pm 0.16$ [93], the LOWZ and CMASS galaxy samples of Data Release 11 of the Baryon Oscillation Spectroscopic Survey (BOSS- LOWZ) and BOSS-CMASS: $D_v(z_{\rm eff} = 0.32)/r_s =$

8.47 ± 0.17 and $D_v(z_{\rm eff} = 0.57)/r_s = 13.77 \pm 0.13$, respectively [94].

2.2.6 Hubble space telescope measurement

In our analyses, we also include Hubble constant measurement from HST as a supplementary probe to the main Planck-CMB data. We use the measurement of present Hubble parameter from low redshift via cosmic distance ladder. This direct and local measurement of H_0 is about 3.4σ far away from the value of $H_0 = 66.93 \pm 0.62$ Km s^{-1} Mpc^{-1}, extrapolated from Planck-CMB measurement within the framework of standard ΛCDM model [32]. The earlier determination of the Hubble constant from HST [95] was $H_0 = 73.8 \pm 2.4$ Km s^{-1} Mpc^{-1} with systematic errors, corresponding to a 3.3% uncertainty. This large uncertainty has been reduced from 3.3% to 2.4% by using the Wide Field Camera 3 (WFC3) on the HST, and also by other improvements. In this thesis work, we use recent 2.4% determination of local value of Hubble constant, $H_0 = 73.24 \pm 1.74$ Km s^{-1} Mpc^{-1} from HST measurement [39]. Recently, an improved local measurement of the Hubble constant, $H0 = 73.48 \pm 1.66$ Km s^{-1} Mpc^{-1} using distance ladder technique from HST is reported in [96], which is 3.7σ far away from Planck-CMB measurement of H_0. The year-wise measurement of H_0 from different measurements is shown in Figure 2.3, where the vertical bars represent errors in the measurements. The figure is extracted from the ESA webpage [97].

2.2.7 Large scale structure probes

The large scale probes provide strong tools to understand the abundance of present matter density and the density fluctuations in the Universe.

1. Planck Sunyaev-Zel'dovich survey

The Sunyaev-Zel'dovich effect [98] is defined as the inverse Compton scattering of CMB photons by the hot gas along the line of sight. This becomes important when the line of sight passes through a galaxy cluster. The galaxy cluster counts are the powerful tools applicable in SZ surveys performed by Atacama Cosmology Telescope (ACT) [99], the South Pole Telescope (SPT) [100] and Planck satellite. The number of clusters and their

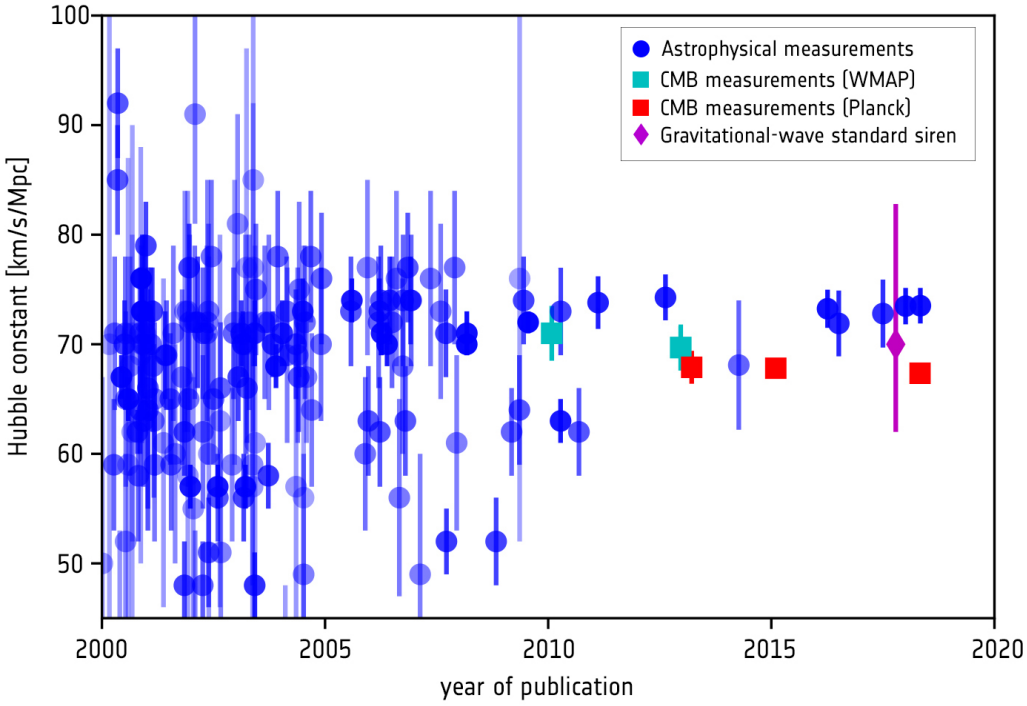

Figure 2.3: Year-wise measurement of H_0 from various measurements as mentioned in the legend.

evolution is very sensitive to today's matter density and the present amplitude of density fluctuations, characterized by σ_8. Also, it is known that primary CMB anisotropy provides the fluctuation at the time of recombination. Therefore, the difference of the fluctuation at two epochs can be treated as a test for the evolution of the perturbation from the time of recombination till today. A detailed description of Planck-SZ measurement and related physics can be seen in [43]. In this thesis work, we use the following constraint:

$$S_8 \equiv \sigma_8 \left(\frac{\Omega_m}{0.27}\right)^{0.30} = 0.782 \pm 0.010$$

2. Canada-France-Hawaii telescope lensing survey

CFHTLenS is the largest weak gravitational lensing survey. It provides a way to understand gravitational deformations in the images of the distant galaxies due to the cosmic LSS. The coherent image distortions, detected in the observed images of galaxies, can be

measured only statistically by averaging over many sources. The weak lensing signal as a function of redshift is sensitive to the growth of structure, and hence indirectly sensitive to the expansion of the Universe as well as the gravitational attraction of various matter density components of the dark sector like DM, DE, neutrinos, etc. In this thesis work, we employ the following constraint from CFHTLenS, weak lensing survey [42]:

$$S_8 \equiv \sigma_8 \left(\frac{\Omega_m}{0.27}\right)^{0.46} = 0.774 \pm 0.040.$$

3. Kilo degree survey-450

The weak gravitational lensing provides a promising way to understand the spatial and temporal distribution of the matter densities of various components of the dark sector. However, the tiny coherent image distortions of background sources caused by the differential deflection of light by foreground masses can only be studied statistically for a large number of sources. Hence, wide-field surveys covering large volume of sky are required for improving the precision of the lensing measurements. For more detailed information about the weak lensing measurements, we refer the reader to see [45, 101, 102]. In this thesis work, we use the following constraint from KiDS-450 [44]:

$$S_8 \equiv \sigma_8 \left(\frac{\Omega_m}{0.27}\right)^{0.50} = 0.651 \pm 0.058.$$

2.3 Methodology

We implement the constructed models in Boltzmann solver code CLASS which is interfeced with parameter inference code Monte Python. From Monte Python code which is based on Metropolis-Hastings algorithm, a Monte Carlo Markov Chain sampling technique, to get MCMC samples on the model parameters. We choose flat (uniform) prior to all the standard ΛCDM parameters as well as extended model parameters in the whole work of the thesis. We use the Planck-CMB 2015 data as the main data set together with some supplementary geometric and LSS probes (as discussed above) in various combi-

nations. To check the convergence of the Monte Carlo Markov Chains, we use Gelman-Rubin criterion [103], according to which $1 - R$ should be less than 0.03 (ideally 0.01), for all the model parameters. For analyzing the obtained samples, we use the Python package GetDist. In the following two subsections, we have given a brief detail about the CLASS and Monte Python codes, and the minimal set of parameters of standard ΛCDM model, their respective values from Planck 2018 results.

2.3.1 CLASS and Monte Python

CLASS [67] is a well-known Boltzmann solver code written in scientific language 'C', and is commonly used by the cosmological community. It is very flexible, user-friendly and freely available for users. It can be easily generalized to implement any non-minimal extension of the ΛCDM model. It is used for parameter estimation of various cosmological models, and also to produce various types of power spectra. This code is refined and updated from time to time with the implementation of new cosmological theories by the team of code developers. In my thesis work, we have used the latest version-2.6.3 and version-2.7.1 of CLASS code. Monte Python [65] code is written in high-level language Python, easy to read and modify, and interfaced with Boltzmann solver code, CLASS. It is based on MCMC sampling: Metropolis-Hastings algorithm, used for parameter inference in cosmology. The Monte python code is designed with the option to use different sampling techniques (usually called methods in code), to explore the parameter space. These include Metropolis-Hastings (default method), Nested Sampling, Cosmo Hammer, etc. Monte Python is inbuilt with predefined likelihoods of many cosmological data sets, and one can define new likelihoods by adding only a few lines in Python. The format of output chains produced by Monte Python code is the same as the format of output chains produced by the CosmoMC code. Therefore, these samples can be analyzed by the GetDist python package or with any other customized code.

2.3.2 Minimal parameter set of the ΛCDM model

The minimal parameter set for a spatially flat (curvature, $k = 0$) ΛCDM model is given as

$$\mathcal{P}_{\Lambda\mathrm{CDM}} = \{\omega_{\mathrm{b}},\, \omega_{\mathrm{cdm}},\, \theta_{\mathrm{s}},\, A_{\mathrm{s}},\, n_{\mathrm{s}},\, \tau_{\mathrm{reio}}\}. \tag{2.28}$$

Here, $\omega_{\mathrm{b}} \equiv \Omega_{\mathrm{b}}h^2$ is today's physical baryon density; $\omega_{\mathrm{cdm}} \equiv \Omega_{\mathrm{cdm}}h^2$ is today's physical cold DM density; θ_{s} is the ratio of sound horizon and the angular diameter distance at decoupling. A_s and n_s, both are perturbative parameters representing the amplitude of primordial scalar perturbations (sometime also called primordial curvature perturbations) at pivot scale $k_\star = 0.05$ Mpc^{-1} and scalar spectrum power-law index (or tilt of the primordial spectrum) at pivot scale $k_\star = 0.05$ Mpc^{-1}, respectively, and τ_{reio} is the optical depth to reionization. The parameters can be re-scaled in order to avoid large steps in the computation and save computation time. This minimal set of parameters is constrained by Planck CMB data alone, and also together with other complementary probes such as BAO, HST, etc. to reduce error bars and to remove degeneracy between parameters. The constraints at 68% CL on six baseline parameters from the latest Planck-CMB [88] (2018) data are displayed in the Table 2.1. Other cosmological parameters are related to

Parameter	Planck (TT,TE,EE+LowE+Lens)
ω_{b}	0.02237 ± 0.00015
ω_{cdm}	0.1200 ± 0.0012
$100\,\theta_{\mathrm{s}}$	1.0411 ± 0.0003
$\log(10^{10}\,A_{\mathrm{s}})$	3.044 ± 0.014
τ_{reio}	0.0544 ± 0.0073
n_{s}	0.965 ± 0.004

Table 2.1: Constraints on the parameters of ΛCDM model at 68% CL from Planck-2018 final release.

these six baseline parameters and hence can be derived with the help of these parameters. The constraints on some derived parameters at 68% CL from Planck CMB 2018 are given

below. The fractional matter density reads

$$\Omega_{\rm m} = \Omega_{\rm b} + \Omega_{\rm cdm} = 0.3153 \pm 0.0073,$$

which immediately gives the fractional DE density (in case of spatially flat Universe)

$$\Omega_{\Lambda} = 0.6847 \pm 0.0073.$$

The present Hubble parameter and amplitude of present matter density fluctuation are respectively given as

$$H_0 = 67.36 \pm 0.54\,{\rm Km\,s^{-1}Mpc^{-1}}, \quad \text{and} \quad \sigma_8 = 0.811 \pm 0.006.$$

Some additional free parameters of this concordance model are kept fixed to their standard (default) values, but in principle they can be varied to extend the base model. An incomplete list of such free parameters include equation of state of DM ($w_{\rm dm} = 0$, default value) and DE ($w_{\rm de} = -1$, default value); sum of the neutrino mass ($\sum m_{\nu} = 0.06$eV, default value); effective number of relativistic species ($N_{\rm eff} = 3.046$, default value); and spatial curvature ($\Omega_{\rm k} = 0$, default value). In this thesis work, the spatial curvature is set to its default value, $\Omega_{\rm k} = 0$ since it is supported by many observations. The possible extensions of the standard ΛCDM model, which are investigated in this thesis work and will be discussed in detail in forthcoming chapters, are briefly explained below. In the next chapter (Chapter 3), we investigate a coupling between DM and photons where the DM decays into photons throughout the cosmic expansion history of the Universe in the presence of a constant as well as a time-varying DE equation of state via Chevalier-Polarski-Linder (CPL) parameterization. In Chapter 4, we study extended or generalized DM parameters: a time-varying equation of state of DM with a constant non-zero sound speed in the presence of a cosmological constant type DE as well as a time-varying DE equation of state via CPL parameterization. In Chapter 5, we investigate a non-gravitational coupling between dark sector components: DM and DE.